> REPLACE THIS LINE WITH YOUR MANUSCRIPT ID NUMBER (DOUBLE-CLICK HERE TO EDIT) <

Investigation of the Long-Term Stability of a Local Oscillator Generator based on InP-Si₃N₄ Laser Source for Satellite Payloads

Alberto Zarzuelo, Jessica César, Robinson Guzmán, Luis González, Charoula Mitsolidou, José Manuel Delgado Mendinueta, Roelof B. Timens, Paulus W. L. van Dijk, Chris G.H. Roeloffzen, Fernando Martin and Guillermo Carpintero

Abstract—**We report an experimental characterization of the long-term stability of a local oscillator (LO) signal generation module for satellite communications based on the optical heterodyning of two InP/Si₃N₄ hybrid integrated lasers. Specifically, we analyze simultaneously the wavelength drift of both lasers in the optical domain and the electrical drift of the generated radiofrequency (RF) beat between the lasers. We identify the main factors that contribute to the overall drift such as the electrical noise coming from the supply sources, the thermal noise coming from the temperature control unit, and the thermal crosstalk between lasers. This investigation compares the stability of an RF signal generated by two approaches. Using two integrated lasers and using a combination of one integrated laser with one external laser. This work also analyzes the difference when lasers are mounted over a standard breadboard with a thermally-controlled. The results show that the best approach is to use both integrated lasers on the same chip. We report a 25 GHz RF signal with long-term stability of 30 MHz measured over 10 hours under free-running operation mode. Moreover, we experimentally demonstrate that integrated lasers can be stabilized by using injection locking. We experimentally demonstrate the optical injection locking of two hybrid InP/Si₃N₄ lasers when the leader laser and the follower laser are both hybrid integrated lasers of same system on chip. When the laser is locked, we report a locking range of 1.86 GHz.**

Index Terms— **Broadband communication, microwave photonics (MWP), millimeter-wave integrated circuits, photonic integrated circuits (PIC), semiconductor lasers.**

S atellite telecommunications aim to push forward their capacity to address the ever increasing demand for higher mobile network data rates. One option to achieve this is to use higher carrier frequencies in the microwave or millimeter-wave range, where there is available bandwidth. However, an increase in capacity is usually associated with an increase in size, mass, and power consumption (SWaP). In satellite communications (SATCOMs) [1], this has become a challenge for the novel Very High Throughput Satellites

(VHTS), where new technologies are required to increase the capacity and flexibility of the communication payloads [2]. Microwave Photonics (MWP) is a promising technology to overcome this challenge because it enables the handling of wider bandwidths as well as increasing the system agility while simultaneously maintaining a low SWaP. A number of research papers have reported high-level architectures of how a photonic payload may look like. Fig. 1 shows a diagram of a satellite photonic payload, where three main blocks (colored green) can be identified:

1) The Photonic Frequency Generation Unit (PFGU), which is mainly the generation and distribution of the optical local oscillator (LO) signal throughout the system.
2) The Photonic multi-frequency converter (PMFC) which combines the optical LO with the RF input data coming with the beams.
3) The Optical Switching Matrix (OSM) makes the optical signal processing as de/multiplexing channels.
4) The Opto-Electronic Module (OEM) to perform the optoelectronic conversion providing RF end-to-end.

According to the Shannon-Hartley theorem, to increase the capacity the bandwidth needs to increase for the same amount of signal and noise powers. That translates into moving the carrier frequencies to higher frequency bands from the current X-band (8-12 GHz) to the Ka (24-40 GHz), Q (33-50 GHz), or V bands (40-75 GHz) [3], which is enabled by the PFGU module. The use of these high frequency bands has been challenging for conventional satellite approaches. Nevertheless, MWP can handle higher data rates and higher frequencies [4] with reduced footprint, low mass, immunity to electromagnetic interferences (EMI), and easier harness routing [5] and [6]. A wide range of applications use MWP technologies to generate radiofrequency (RF) signals. So far, MWP systems and links have relied almost exclusively on discrete components [7], which negatively impacts their

Alberto Zarzuelo, Jessica Cesar, Luis Gonzalez, José Manuel Delgado Mendinueta and Guillermo Carpintero are with the Carlos III University of Madrid, 28911 Madrid, Spain (email: azarzuel@pa.uc3m.es; jecesarc@ing.uc3m.es; lgguerre@ing.uc3m.es; jodelgad@ing.uc3m.es; guiller@ing.uc3m.es).

Robinson Guzmán is with the Universidad Rey Juan Carlos, 28942, Madrid, Spain (email: robinson.guzman@urjc.es)

Charoula Mitsolidou, Roelof B. Timens, Paulus W. L. van Dijk and Chris G.H. Roeloffzen are with Lionix International B.V, 7521 AN Enschede, The Netherlands (email: c.mitsolidou@lionix-int.com; r.b.timens@lionix-int.com; c.g.h.roeloffzen@lionix-int.com; p.w.l.vandijk@lionix-int.com)

Fernando Martin is with SENER Aeroespacial S.A.U, 28760 Tres Cantos, Madrid (email: fernando.martin@aeroespacial.sener)

volume and mass-producing in bulk, increases costs, and is power-hungry [8]. Recently, photonic integration technology has been introduced, coining the term integrated microwave photonics (iMWP), which enables a significant improvement in terms of size, weight, and power consumption [9]. In addition, RF signals generated using photonic sources integrated on a photonic integrated circuit (PIC) may have additional advantages which greatly depend on the RF signal generation technique [10], often based either on short pulse laser sources or on optical heterodyning [11].
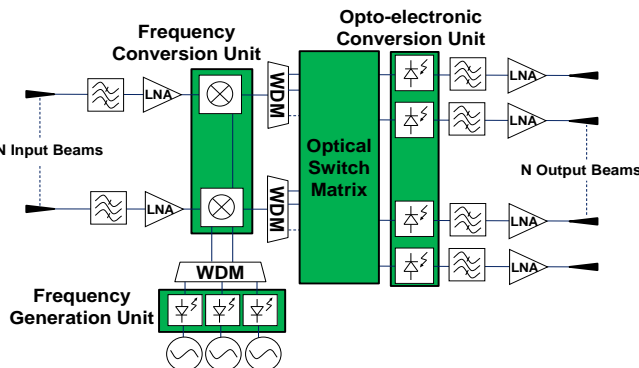

Fig. 1. High-level scheme of a satellite photonic payload.

There are various techniques for photonic-based RF generation. Among them, optical heterodyning offers the highest flexibility in terms of tunability and wider tuning ranges [12]. This technique is based on the combination of two semiconductor tunable lasers on an O/E converter with enough bandwidth to produce a beat note defined by the wavelength spacing of frequency offset between the lasers. The most common approach for the light source is to use a dual-wavelength source that includes two single-frequency lasers, where one of the lasers can be wavelength-tunable or alternatively both lasers [13] for higher flexibility. The beat note RF signal can range from a few MHz up to the THz range, which is far beyond the conventional RF LO generators [14]. However, the main disadvantage of this approach happens when the integrated lasers operate under the free-running condition, resulting in a large phase noise of the beat note and a long-term drift of the beating frequency [15]. Even when both lasers may have very low linewidths of less than 1 kHz, the RF beat-note still may exhibit a long-term drift mainly produced by three factors: 1) the electrical noise coming from the electrical power sources, and 2) the thermal noise originating from the thermal feedback control loop and 3) the thermal cross-talk within the integrated device [16]. To overcome this problem, several solutions have been proposed. The most usual is to add a stabilization system such as optical injection-locking (OIL) [17]-[18], using an optical frequency comb generator or an optical phase-locked loop (OPLL) [19]-[20]. The main disadvantage of this approach is the increase in complexity and SWaP due to the addition of additional elements to the subsystem. This solution usually requires an external laser source for the frequency comb generation. An integrated approach mitigates this increase by using an integrated light source as a reference for the comb generation and avoids the

necessity to use a bulky light source. There are several examples reported in the literature of on-chip optical injection locking [21]-[22]. Nevertheless, in those works the optical injection was performed in a monolithic InP platform where the propagation losses are in the range [1, 3] dB/cm, as documented in the Process Design Kits (PDKs) provided by the foundries. In contrast, a hybrid InP/Si_3N_4 technology has a propagation loss as small as 0.01 dB/cm [23]. This enables higher-performance passive components, such as optical filters and splitters, which are the main building blocks, i.e., OSM, in satellite payload schemes. Moreover, this platform has reported the narrowest fundamental laser linewidth of 290 Hz with a widest-ever spectral coverage spanning 81 nm with a central wavelength of 1550 nm [24].

The purpose of this paper is to experimentally evaluate the feasibility of using photonic integrated light sources for the generation of an RF LO that can operate in the microwave domain. The paper will focus on the frequency stability of the generated RF signal as a key parameter. The main factors that contribute to a reduction of long-term stability will be analyzed among different approaches and scenarios. We conclude that the best approach for improving the frequency stability is to have both photonic sources integrated on the same chip. A 20% improvement in the overall optical drift has been reported by using a water-cooled breadboard as a temperature-controlled heat sink. RF drift of 30 MHz measured over 10 hours has been demonstrated. Finally, this work carries out a stabilization technique based on optical injection locking to mitigate the optical drift demonstrating an optical injection locking of one integrated laser using another laser integrated on the same chip. As a figure of merit, a locking range of 1.86 MHz has been reported which is above 3 times higher than the worst-case of optical drift measured.

The rest of the paper is divided into the following sections. Section II describes the two photonic devices that have been characterized during the course of this work. Section III focuses on the characterization of the devices and the comparison in terms of frequency stability. Section IV describes an experiment of optical injection locking that can be potentially used to stabilize the lasers under one single reference. Finally, Section V draws the conclusions and the future lines of work.

II. DESCRIPTION OF THE PHOTONIC DEVICES

Two devices were used for the experimental characterization. Firstly, a custom-integrated dual laser source was supplied by the company LioniX International and secondly, a commercially available compact laser module was supplied by the company Chilas.

The LioniX hybrid integrated dual laser module investigated in this work is shown schematically in Fig. 2. Each laser cavity is formed through hybrid integration of an InP Quantum-Well (QW) gain chip (red boxes) and a Si_3N_4 chip (gray shaded area) using butt-coupling. The chip size is 15x10 mm. A picture of the assembly is shown in Fig. 3. The InP gain chip is a double-pass reflective semiconductor optical amplifier (RSOA) through high-reflective (HR) coating on the leftmost
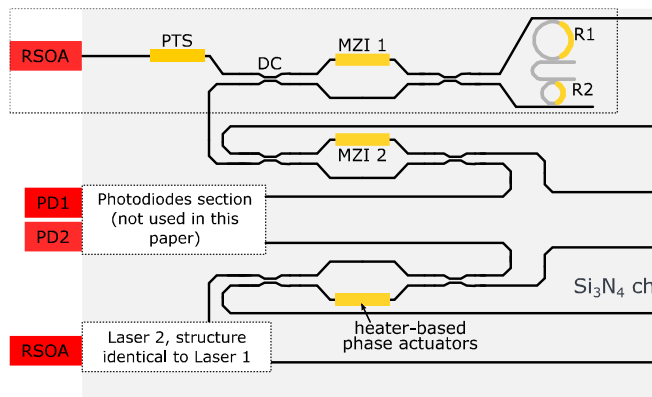
Fig. 2. Block diagram of the LioniX hybrid dual laser module: gain sections, ring resonators, AMZI and directional couplers.

Fig. 3. LioniX dual hybrid InP/Si$_3$N$_4$ laser assembly

edge, which forms one of the cavity mirrors. The other mirror is an integrated mirror structure in the Si$_3$N$_4$ substrate, based on a pair of micro ring resonators (R1 and R2) which provide a wavelength tunable optical feedback. The two MRRs have a Free Spectral Range (FSR) of around 1.6 nm (200 GHz), with slightly different radiuses to enable wavelength tuning owing to the Vernier effect [25]. In between the two mirrors, the lasers include a thermally adjustable Phase Tuning Section (PTS) and a 2x2 symmetric Mach-Zehnder Interferometer-based Thermo-Optic Power Coupler (MZI-TOPC) [26] which allows control of the amount of light fed back to the laser cavity. The Si$_3$N$_4$ waveguides, having a symmetric double-stripe cross-section, offer a low propagation loss of about 0.1 dB/cm [27], which allows MRRs to reach Q-factors ranging from 20,000 to 3,000,000 [28]. Each laser has an additional I/O control MZI-TOPC which allows to control the amount of the laser optical power that is directed either to the on-chip photodiodes or to an output optical fiber. Finally, the on-chip photodiodes include another MZI-TOPC, which allows to control the amount of power from each laser that is directed toward each on-chip photodiode, PD1, and PD2. The optical waveguide access ports are coupled to single-mode polarization-maintaining fibers, which are terminated with an angled facet FC/APC connector to avoid back-reflections into the laser cavity. The gain sections of the lasers have a power consumption of 500 mW when both lasers output the maximum allowed optical power. The heater-based actuators for the RR and the MZI-TOPC have an average power consumption of 350 mW. The chip is mounted over a

dedicated assembly with DC access pads and coupling points to a fiber array. The size of the whole assembly is 80x40 mm.

Chilas laser module is schematically shown in Fig. 4. This laser comprises an InP reflective semiconductor optical amplifier (RSOA) as a gain medium and a Si$_3$N$_4$ waveguide circuit as a tunable external cavity. The RSOA is butt-coupled to the external cavity. On the left-hand side, there is a gain section which is high-reflective on the left-hand side, and anti-reflective on the right-hand side where it is connected to a TriPleX^{TM} Silicon Nitride external cavity waveguide chip. The external cavity has two coupled micro-ring resonators (MRRs) with slightly different FSRs in the cavity to ensure stable single-frequency operation by the Vernier effect. On the SiN chip, there are 5 heaters positioned, one to control the phase of the light in the cavity, two to control the resonant wavelengths of the ring resonators Ring 1 (R1) and Ring 2 (R2), which controls the output wavelength, and two control the optical power coupled out of the cavity. The laser's frequency can be tuned over a large range by means of tuning the MRR. A picture of the device is shown in Fig. 5. The power consumption is approximately 1 W, as one of the lasers of the LioniX hybrid module. The laser is mounted on a 14-pin butterfly assembly with a total size of 13x30 mm.
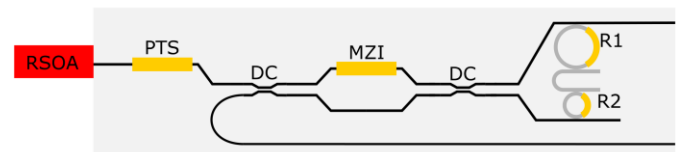

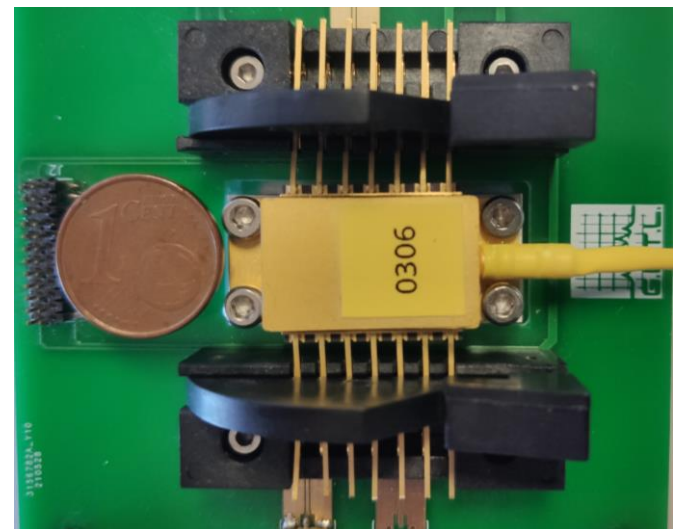**Fig. 4**. Schematic of Chilas laser

Fig. 5. Chilas laser is integrated in a 14-pin butterfly package.

III. EXPERIMENTAL CHARACTERIZATION OF THE PHOTONIC DEVICES

The InP/Si$_3$N$_4$ hybrid integrated dual laser module was assembled in a custom alumina base. A Peltier module was placed below the area of the chip. The feedback loop was closed using the thermoelectric cooler (TEC) control and negative temperature coefficient (NTC) thermistor close to the chip. The module

operated between 20°C and 22°C throughout all the reported measurements. The current injected on the gain section RSOAs is driven from custom battery supply current sources, to reduce the electrical noise, while the heaters in the chip, one per each Mach-Zehnder Interferometer-based Thermo-Optic Power Coupler, as well as the heaters from the MRRs, are driven from low-noise voltage sources, Keysight E3611.

The Chilas laser is integrated into a 14-pin butterfly package, enabling compatibility with any standard 14-pin laser diode mount. The laser contains an integrated thermoelectric cooler (TEC), thermistor. The module operated between 20°C and 22°C as well. The current injected on the gain section SOAs and the TEC controller was driven by a commercially available current and TEC source, ILX-Lightwave LDC-3724B. We saw that daily temperature fluctuations and the day-night temperature cycles affect the devices. Both devices were covered with a homemade insulation box in order to protect the devices from environmental conditions and keep the temperature constant. The devices were working at a laboratory temperature of 25 °C, where the temperature was supposed to be stable.

A. Characterization of one integrated laser with one external laser (1st approach).

For this approach, the integrated module from LioniX and the external laser from Chilas was tested simultaneously. Fig. 6 shows the optical spectrum of the lasers. Lasers were biased in such a way that the frequency difference between LioniX Laser 1-LioniX Laser 2 was set at 34.5 GHz. The frequency difference between Lionix Laser 2-Chilas was set at 41.6 GHz. By this way, the RF beat notes can be tested simultaneously, as both frequencies were within the photodiode bandwidth. Fig. 7 shows the temporal evolution of the optical and electrical drift measured over a period of 10 hours. In order to maintain the balance between the optical powers of the lasers, the current of SOA sections was set at 60 mA. PTS and MZM heaters of LioniX laser 1 were biased at 8.68 V and 13.68 V, respectively.
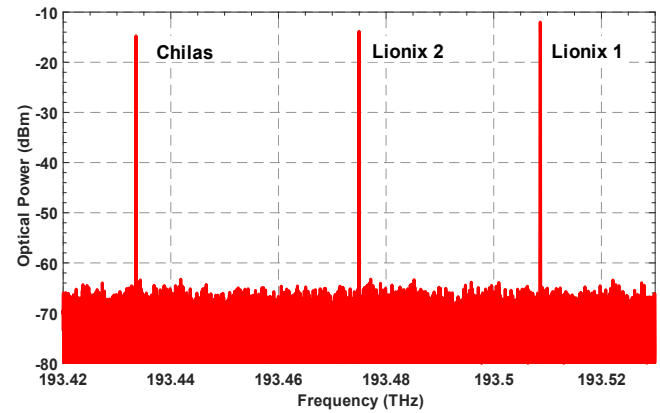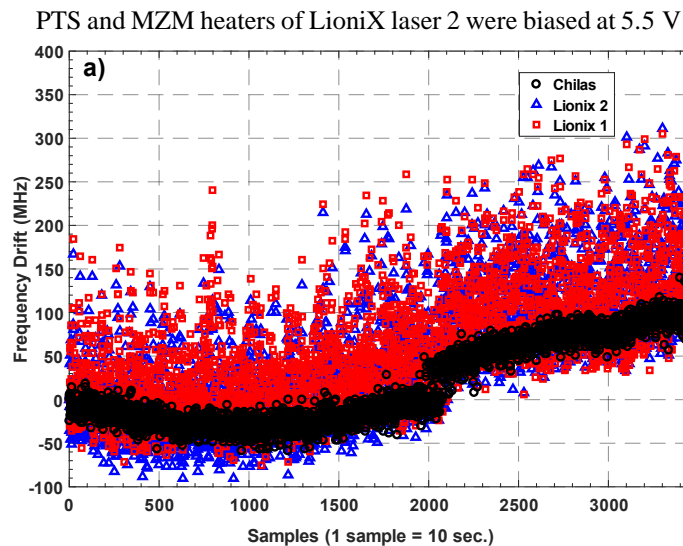
PTS and MZM heaters of LioniX laser 2 were biased at 5.5 V

Fig. 6. Optical spectrum of the LioniX hybrid integrated dual laser and the Chilas laser emitting simultaneously.

and 13.55 V, respectively. The heaters that control the wavelength tuning, R1 and R2, were biased with 0 V and 13.185 V, respectively for LioniX laser 1 and LioniX laser 2. To the best of our knowledge, the main reason could be the change in the amount of heat generated by the device to be compensated by the thermal control unit. Regarding the external laser, we can observe an optical drift was approximately 150 MHz. Fig. 7 (c) shows the RF drifts of the beating between Laser 1 and Laser 2. There is an anomalous behavior between the samples 500 and 1000. This behavior was the result of a mode-hope due to the tuning mechanism being based on Vernier effect. Assuming this fact, we concluded that the electrical drift of the generated RF frequency between Laser 1-Laser 2 was around 30 MHz, while the electrical drift produced of the RF tone generated by Laser 2-Chilas was around 300 MHz, as shown in Fig. 7 (b). If we compare the traces of Fig. 7 (b) and (c), there was a notable increase in the electrical drift of the RF frequency generated between the integrated Laser 1 and Laser 2 and Chilas with Laser 2. Although the Chilas laser was more stable by itself, Fig. 7 (a), the fact of using two different thermal controllers for each device means that there is no correlation between the thermal compensation produced by the TEC units to keep the same
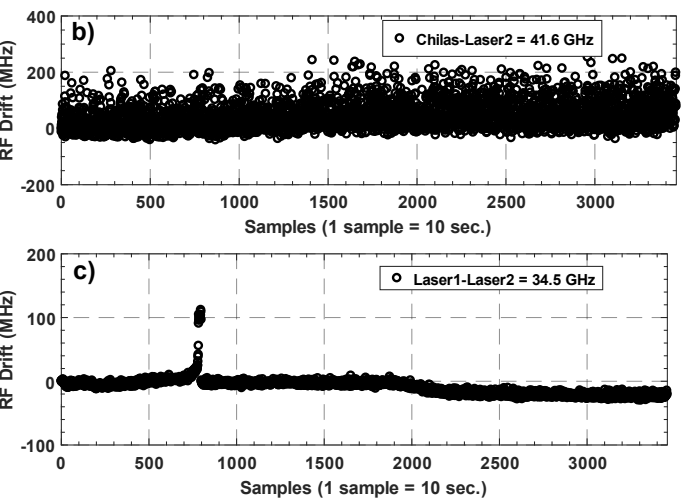

Fig. 7. Temporal evolution InP/Si$_3$N$_4$ hybrid integrated dual laser and Chilas laser drift measured over a period of 10 hours. (a) Optical spectrum of Laser 1, Laser 2 & Chilas laser; (b); RF beat note signal at 41.6 GHz between Chilas and Laser 2. (c). RF beat note signal at 34.6 GHz between Laser 1 and Laser 2.

temperature. This fact produces an increase in the RF drift when we beat the integrated Laser 2 with the Chilas.

B. Characterization of two integrated lasers over a water-cooled breadboard (2nd approach).

In this experiment, the idea was to provide a fully controlled thermal environment to reduce the thermal fluctuations that can negatively affect the system. A water-cooled breadboard was added for this purpose. PTS and MZM 1 heaters were biased at 13.632 V and 13.55 V, respectively. The temperature of the water-cooled breadboard was adjusted by a Chiller and set to 21ºC. The current injected into the gain section was 40 mA. The bias point of R1/R2 heaters was set at 11.18 V to keep a wavelength difference of 25 GHz. Fig. 8 shows the temporal evolution of the drift measured over 10 hours (a) optical drift and (b) RF drift. The optical drift reported in the 1st approach was 500 MHz while in this experiment the drift was around 100 MHz. A reduction of 80%.
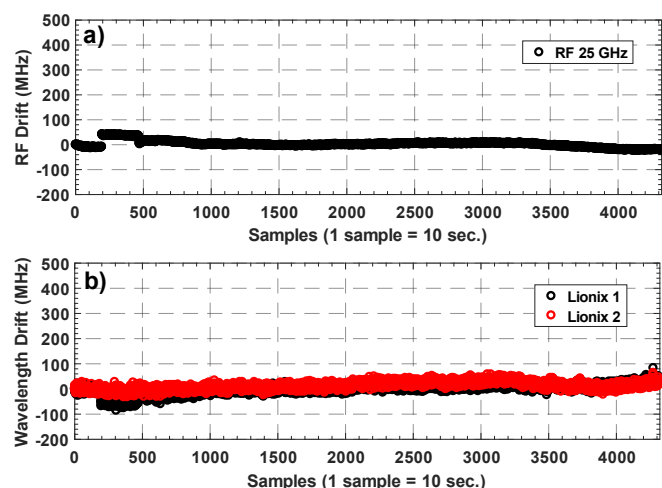

Fig. 8. Temporal evolution of InP/Si$_3$N$_4$ hybrid integrated dual laser drift using water-cooled breadboard measured over a period of 12 hours. (a) RF drift of the generated RF frequency at 25 GHz. (b) Optical drift of each laser.

The reduction was produced by two factors. Using a lower current injected to feed the gain sections reduce the electrical noise introduced in the devices by the gain sections. The second factor is due to the water-cooled breadboard providing a thermally controlled heat sink. When the device was heated up, the gradient that the Peltier needed to generate is less, so it consumed less power reducing the noise.

If we compare the RF drift between Fig. 8 (a) and Fig. 7 (c), it can be noticed that the behavior was quite similar. In Fig. 7 (c) the RF drift was around 30 MHz. In Fig. 8 (a), the RF drift was 30 MHz as well, over the same period. This factor can also be seen in Fig. 9, where the phase noise of the RF beat note was measured with the standard optical breadboard and with the water-cooled breadboard. The behavior was similar. The phase noise was approximately - 92 dBc/Hz at 100 kHz. This result matched what we saw in Fig. 8 and Fig. 7.
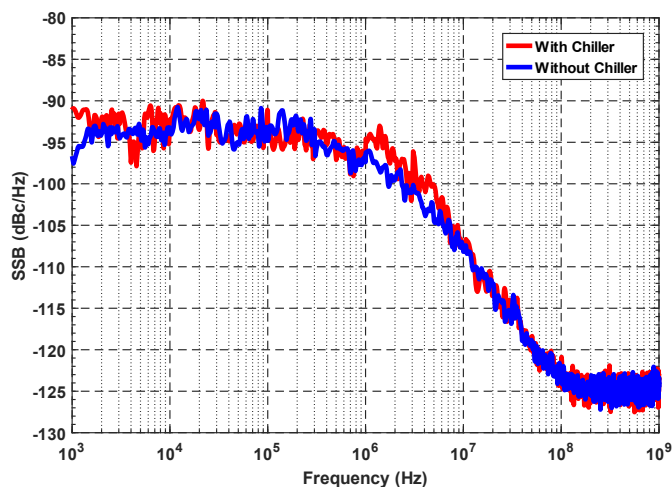

Fig. 9. Phase noise measurement of the generated RF beat note. (red trace) with Chiller. (blue trace) without Chiller

IV. OPTICAL INJECTION LOCKING EXPERIMENT USING INTEGRATED LASERS.

Measuring the free-running drift is key as it determines the minimum locking range (and, hence, injection ratio) required to maintain the OIL. For this experiment, Laser 1 acted as the follower laser and Laser 2 was the leader laser. RSOA section of Laser 1 was supplied with 90 mA. The optical power was 0 dBm. The experimental setup is shown in Fig. 10. The output light from the LioniX laser 2 is sent to an optical circulator to optically inject the light of the LioniX laser 1 while avoiding any back-reflections. Before the circulator, a 99/1 optical splitter is included to measure the optical power output by LioniX laser 2. Based on the optical power monitoring, the optical power injected from the leader laser to the follower laser is -3 dBm.

Therefore, for this experiment, an Injection Ratio of -3 dB was used. The optical outputs of both the leader laser and the follower laser were connected to a high-resolution optical spectrum analyzer. Hence, the optical spectrum of each laser can be measured separately, and also when injection locking is performed.
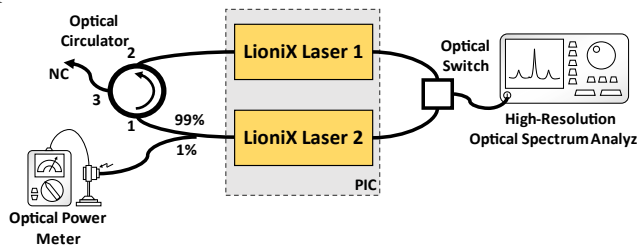

Fig. 10. Experimental setup of the injection locking experiment between hybrid InP/Si$_3$N$_4$ integrated lasers on the same chip.
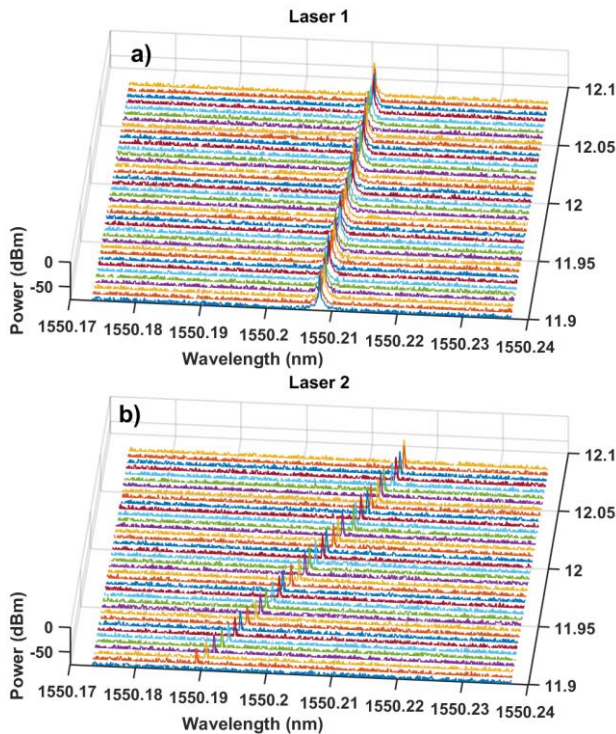
Fig. 11. (a) Optical spectrum of Laser 1 when sweeping R1/R2. (b) Optical spectrum of Laser 2 when sweeping R1/R2.

Heater MZI 1 was biased at 13.632 V. In this way, the MZM was connected in through and the amount of light passing from laser 2 to laser 1 is maximized. Heaters R1 and R2 of the follower laser were biased at zero volts to keep the wavelength fixed, Fig. 11 (a). Heaters R1 and R2 heaters of the leader laser were swept in a voltage range between 11.09 V to 12.09 V. Over this range, a spectral region where the leader laser can be continuously tuned above the follower laser was founded, Fig. 11 (b).

As Laser 2 got close to Laser 1 we appreciate intermodulation products appeared, Fig. 12. This occurs when the follower laser was out of the locking range of the leader laser. Intermodulation products got stronger as the voltage applied to R1/R2 got near 11.96 V. When locking was achieved at a voltage of 11.99 V, a clean signal was visible. The follower laser remained locked up to a voltage of 12.1 V. At this point, the intermodulation phenomena appeared again. That means that the laser is not locked anymore. A locking range of 1.86 GHz was achieved. This value 3 times higher than the worst case of drift reported at the 1st approach. Even in that case, we ensure that the laser will be stabilized.
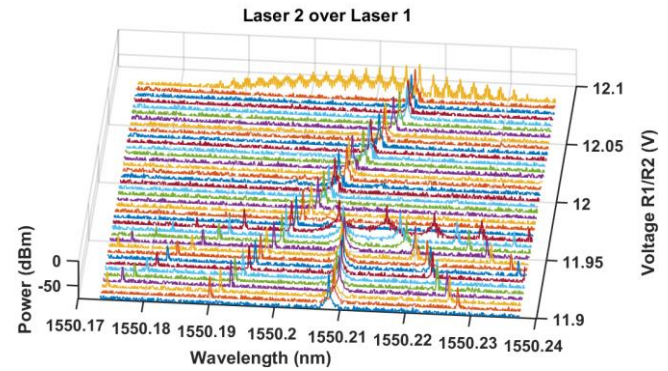

Fig. 12. Optical spectrum of the injection locking experiment. Laser 2 injects over Laser 1 while R1/R2 are swept from 11.9 V to 12.1 V

V. CONCLUSIONS

In this paper, we have presented a study of the stability of a dual-integrated laser module. We have measured the optical drift and the RF drift of the generated beat-note signal. The lasers exhibited an optical drift up to 500 MHz and an RF drift of around 30 MHz. We have introduced an external laser to see if the stability of the RF beat-note is improved. We report an optical drift of 150 MHz. However, the stability of the RF signal was better from the beating between the integrated lasers. The RF drift of the signal that comes from the beating of the integrated lasers was around 30 MHz, while the RF drift of the signal that comes from the combination of one integrated laser and the external laser was around 300 MHz. This behavior is due to the fact that lasers are integrated on the same chip. The chip uses a unique thermal controller. The temperature compensation of the thermal fluctuations is very similar on each laser. The frequency shifts due to the thermal control were correlated. We have analyzed the impact of the surface where the chip is mounted. The standard optical breadboard was substituted by a water-cooled breadboard to provide a temperature-controlled heat sink. The optical drift has been improved from 500 MHz to 100 MHz and a reduction of 80% of the overall optical drift has been found. We conclude that the best approach is to have both lasers under the same thermal controller. The electrical RF drift was similar in the two scenarios. Using the standard optical breadboard, the RF drift was around 30 MHz while with the water-cooled breadboard, the RF drift was 30 MHz. This fact was corroborated by measuring the phase noise of the generated RF signal. We report approximately a phase noise of -92 dBc/Hz at 100 kHz for the two scenarios. Additionally, we have experimentally demonstrated the optical injection locking of two hybrid InP/Si_3N_4 lasers using leader laser and follower laser integrated on the same system on chip. We achieved a locking range of 1.86 GHz. This value is above 500 MHz, which is the worst-case optical drift reported in this paper.

In future work, we aim to develop an optical frequency comb by adding an integrated on-chip optical modulator. We hope that the generated RF signal could be stabilized while maintaining a reasonable SWaP which is one of the main targets in this work.

REFERENCES

[1] S. Vono *et. al*., "Towards telecommunication payloads with photonic technologies," in *Proc. SPIE 10563, International Conference on Space Optics (ICSO)*, Chania, Greece, 2018

[2] G. Charalambous and S. Iezekiel, *"*Microwave photonic frequency generation and conversion unit design for Ka-band satellite payloads," *in Proc. SPIE 11852, International Conference on Space Optics (ICSO)*, Online Only, France, 2020.

[3] O. Kodheli *et al*., "Satellite Communications in the New Space Era: A Survey and Future Challenges," in *IEEE Communications Surveys & Tutorials*, vol. 23, no. 1, pp. 70-109, Firstquarter 2021.

[4] A. Stöhr, "Photonic millimeter-wave generation and its applications in high data rate wireless access," *in IEEE International Topical Meeting on Microwave Photonics*, Montreal, QC, Canada, pp. 7-10, 2010.

[5] R. T. Logan Jr., Davinder Basuita, "Mass-reduction of high-speed spacecraft datalinks enabled by rugged photonic transceivers," *Proc. SPIE 11180, International Conference on Space Optics (ICSO)*, Chania, Greece, 2018.

[6] R. T. Logan and D. Basuita, "Photonic components for spacecraft fiber optic datalinks and free-space optical communications terminals," *in Proc. SPIE 11852, International Conference on Space Optics (ICSO)*, Online Only, France, 2020.

[7] G. Carpintero *et. al*., "Photonic Integrated Circuits for Radio-Frequency Signal Generation," in *Journal of Lightwave Technology*, vol. 34, no. 2, pp. 508-515, Jan 15, 2016.

[8] Javad Anzalchi *et. al*., "Towards demonstration of photonic payload for telecom satellites," *in Proc. SPIE 11180, International Conference on Space Optics (ICSO)*, Chania, Greece, 2018.

[9] D. Marpaung *et. al*., "Integrated microwave photonics," *in Nature Photon*, vol. 13, pp. 80-90, Jan, 2019.

[10] T. Nagatsuma *et. al*., "Generation of Low-phase and Frequency-tunable Millimeter-/terahertz waves using Optical Heterodyning Tehcniques with UTC-PD," *in Proc of 36th European Microwave Conference*, Manchester, United Kingdom, 2006.

[11] M. Lo *et. al*., "Monolithically Integrated Microwave Frequency Synthesizer on InP Generic Foundry Platform," *in Journal of Lightwave Technology*, vol 36, no. 19, pp.4626-4632, Oct 1, 2018.

[12] T. Nagatsuma and G. Carpintero, "Recent Progress and Future Prospect of Photonics-Enabled Terahertz Communications Research," *in IEICE Trans. On Electronics*, vol E98-C Issue, pages 12, 1060-1070, 2015.

[13] M. Lo, A. Zarzuelo, R. Guzmán and G. Carpintero, "Foundry-Fabricated Heterodyne DFB Laser Microchip for 600 MHz – 23 GHz RF Generation," *in 48th European Microwave Conference (EuMC)*, Madrid, Spain, pp. 793-795, 2018.

[14] T. Nagatsuma, "Advances in Terahertz Communications Accelerated by Photonics Technologies," *in 24th OptoElectronics and Communications Conference (OECC) and 2019 International Conference on Photonics in Switching and Computing (PSC)*, Fukuoka, Japan, pp. 1-3, 2019.

[15] L. G. Guerrero *et al*., "InP-Si3N4 Hybrid Integrated Optical Source for High-purity Mm-wave Communications," *in Optical Fiber Communications Conference and Exhibition (OFC)*, pp. 1-3, 2022.

[16] M. Milanizadeh, D. Aguiar, A. Melloni and F. Morichetti, "Canceling Thermal Cross-Talk Effects in Photonic Integrated Circuits," in Journal of Lightwave Technology, vol. 37, no. 4, pp. 1325-1332, Feb 15, 2019.

[17] M. J. Fice, A. Chiuchiarelli, E. Ciaramella and A. J. Seeds, "Homodyne Coherent Optical Receiver Using an Optical Injection Phase-Lock Loop," in Journal of Lightwave Technology, vol. 29, no. 8, pp. 1152-1164, April 15, 2011.

[18] E. Sooudi et al., "Injection-Locking Properties of InAs/InP-Based Mode-Locked Quantum-Dash Lasers at 21 GHz," in IEEE Photonics Technology Letters, vol. 23, no. 20, pp. 1544-1546, Oct.15, 2011.

[19] K. Balakier et al., "Optical phase lock loop as high-Q filter for optical frequency comb line selection," *in* International Topical Meeting on Microwave Photonics (MWP), Beijing, China, 2017, pp. 1-4, 2017.

[20] K. Bałakier et al., "Monolithically integrated optical phase lock loop with 1 THz tuneability," *in* 42nd International Conference on Infrared, Millimeter, and Terahertz Waves (IRMMW-THz), Cancun, Mexico, pp. 1-2, 2017.

[21] Perrott AH, Caro L, Dernaika M, Peters FH. A Comparison between off and On-Chip Injection Locking in a Photonic Integrated Circuit. Photonics. 2019; 6(4):103.

[22] A. Tauke-Pedretti et al., "Mutual Injection Locking of Monolithically Integrated Coupled-Cavity DBR Lasers," in IEEE Photonics Technology Letters, vol. 23, no. 13, pp. 908-910, 2011.

[23] C. G. H. Roeloffzen *et al*., "Low-Loss Si3N4 TriPleX Optical Waveguides: Technology and Applications Overview," in *IEEE Journal of Selected Topics in Quantum Electronics*, vol. 24, no. 4, pp. 1-21, July-Aug. 2018, Art no. 4400321.

[24] Y. Fan *et al*., "290 Hz intrinsic linewidth from an integrated optical chip-based widely tunable InP-Si3N4 hybrid laser," *2017 Conference on Lasers and Electro-Optics (CLEO)*, San Jose, CA, USA, 2017, pp. 1-2.

[25] Yang Liu *et. al.*, "Integrated microwave photonic filters," in *Adv. Opt. Photon. 12*, 485-555, 2020.

[26] C.G.H. Roeloffzen et al., "Silicon nitride microwave photonic circuits," *in Opt. Exp*., vol. 21, pp. 22937–22961, 2013.

[27] K. Wörhoff *et al*., "TriPleX: A versatile dielectric photonic platform," *in Adv. Opt. Technol*., vol. 4, pp. 189–207, 2015.

[28] C. Taddei, L. Zhuang, C. G. H. Roeloffzen, M. Hoekman and K. -J. Boller, "High-Selectivity On-Chip Optical Bandpass Filter With Sub-100-MHz Flat-Top and Under-2 Shape Factor," in *IEEE Photonics Technology Letters*, vol. 31, no. 6, pp. 455-458, 15 March15, 2019.